arXiv:astro-ph/0510530v1 18 Oct 2005

The First INTEGRAL AGN Catalog

V. Beckmann[1], N. Gehrels, C. R. Shrader[2]
NASA Goddard Space Flight Center, Exploration of the Universe Division, Code 661, Greenbelt, MD 20771, USA
`beckmann@milkyway.gsfc.nasa.gov`

S. Soldi[3]
INTEGRAL Science Data Centre, Chemin d' Écogia 16, 1290 Versoix, Switzerland

ABSTRACT

We present the first *INTEGRAL* AGN catalog, based on observations performed from launch of the mission in October 2002 until January 2004. The catalog includes 42 AGN, of which 10 are Seyfert 1, 17 are Seyfert 2, and 9 are intermediate Seyfert 1.5. The fraction of blazars is rather small with 5 detected objects, and only one galaxy cluster and no star-burst galaxies have been detected so far. A complete subset consists of 32 AGN with a significance limit of 7σ in the *INTEGRAL*/ISGRI 20–40 keV data. Although the sample is not flux limited, the distribution of sources shows a ratio of obscured to unobscured AGN of $1.5-2.0$, consistent with luminosity dependent unified models for AGN. Only four Compton-thick AGN are found in the sample. Based on the *INTEGRAL* data presented here, the Seyfert 2 spectra are slightly harder ($\Gamma = 1.95 \pm 0.01$) than Seyfert 1.5 ($\Gamma = 2.10 \pm 0.02$) and Seyfert 1 ($\Gamma = 2.11 \pm 0.05$).

Subject headings: galaxies: active — catalogs — gamma rays: observations — X-rays: galaxies — galaxies: Seyfert

1. Introduction

The X-ray sky as seen by X-ray satellites over the past 40 years, shows a substantially different picture than for example the optical band. While the visual night sky is dominated by main sequence stars, Galactic binary systems and super nova remnants form the brightest objects in the X-rays. Common to both regimes is the dominance of active galactic nuclei (AGN) toward lower fluxes. In the X-ray range itself, one observes a slightly different population of AGN at soft and at hard X-rays. Below 5 keV the X-ray sky is dominated by AGN of the Seyfert 1 type, above the absorbed Seyfert 2 objects appear to become more numerous. These type 2 AGN are also the main contributors to the cosmic X-ray background above 5 keV (Setti & Woltjer 1989; Comastri et al. 1995; Comastri et al. 2001; 1), although only ∼ 50% of the XRB above 8 keV can be resolved (Worsley et al. 2005). Beside the rather persistent Seyfert galaxies, also blazars are detectable in the hard X-rays. Because of the fact that we look into a highly relativistic jet in the case of those sources, the blazars exhibit strong variability on all time-scales and are especially variable in the X-ray and high-energy gamma-ray domain. For an overview over the various extragalactic X-ray surveys see Brandt & Hasinger (2005), and for early *INTEGRAL* results see Krivonos et al. (2005).

The hard X-ray energy range is not currently accessible to X-ray telescopes using grazing incidence mirror systems. Instead detectors without spatial resolution like the PDS (Frontera et al. 1997) on *BeppoSAX* (Boella et al. 1997) and OSSE (Johnson et al. 1993) on *CGRO* (Gehrels et al. 1993) have been applied. A synopsis of these previous results is as follows: the $2-10$ keV Seyfert 1 continua are approximated by a $\Gamma \simeq 1.9$ powerlaw form (Zdziarski et al. 1995). A flattening above ~ 10 keV has been noted, and is commonly attributed to Compton reflection (George & Fabian 1991). There is a great deal of additional detail in this spectral domain - "warm" absorption, multiple-velocity component outflows, and relativistic line broadening - which are beyond the scope of this paper. The Seyfert 2 objects are more poorly categorized here, but the general belief is that they are intrinsically equivalent to the Seyfert 1s, but viewed through much larger absorption columns [see e.g. Véron-Cetty & Véron (2000) for a recent review].

---

[1] also with the Joint Center for Astrophysics, Department of Physics, University of Maryland, Baltimore County, MD 21250, USA

[2] also with Universities Space Research Association, 10211 Wincopin Circle, Columbia, MD 21044, USA

[3] also with Observatoire de Genève, 51 Ch. des Maillettes, 1290 Sauverny, Switzerland

Above 20 keV the empirical picture is less clear. The $\sim 20-200$ keV continuum shape of both Seyfert types is consistent with a thermal Comptonization spectral form, although in all but a few cases the data are not sufficiently constraining to rule out a pure powerlaw form. Nonetheless, the non-thermal scenarios with pure powerlaw continua extending to $\sim$ MeV energies reported in the pre-*CGRO* era are no longer widely believed, and are likely a result of background systematics. However, a detailed picture of the Comptonizing plasma - its spatial, dynamical, and thermodynamic structure - is not known. Among The critical determinations which *INTEGRAL* or future hard X-ray instruments will hopefully provide are the plasma temperature and optical depth (or Compton "Y" parameter) for a large sample of objects.

The other major class of gamma-ray emitting AGN - the blazars (FSRQs and BL Lac objects) are even more poorly constrained in the *INTEGRAL* spectral domain. The detection of ~ 70 of theses objects with the EGRET instrument on *CGRO* in the 1990s has established the presence of $\Gamma \sim 10$ relativistic plasma at small angles to the observers line of sight. The so called "TeV" blazars are similar objects but with the peak power shifted to even greater energies, probably due to an even smaller viewing angle (see for example, Fossati et al. 1999, and for earlier *INTEGRAL* results Pian et al. 2005). The most common interpretation of the broad-band continuum emission is the synchrotron self Compton (SSC) model, although the external Compton models (EC) are still also plausible. Broad-band temporal coverage can in principle discriminate between these possibilities, although each of these components can separately contribute to the hard-X-ray band under extreme circumstances. The *INTEGRAL* bandpass covers a critical region which can in principle establish the amplitude and shape of the high-end synchrotron component or or low-end SSC component.

Critical to each of these issues is the need to obtain improved continuum measurements over the hard X-ray to soft gamma-ray range for as large a sample of objects as possible. *INTEGRAL* (Winkler et al. 2003), since its launch in October 2002, offers unprecedented > 20 keV collecting area and state of the art detector electronics and background rejection capabilities. Thus it offers hope of substantial gains in our knowledge of the AGN phenomenon. We were thus motivated at this juncture some three years into the mission, to formulated and present the collective look at the data so far obtained and assess the potential for progress in the *INTEGRAL* era.

As the satellite spent most of its observing time up to now concentrating on the Galactic plane, some low-latitude AGN have been detected. Observations at higher Galactic latitude have also led to studies of individual sources: 3C 273 (Courvoisier et al. 2003a), NGC 4388 (Beckmann et al. 2004), GRS 1734–292 (Sazonov et al. 2004), the S5 0716+714 field (Pian et al. 2005), PKS 1830–211 (De Rosa et al. 2005), NGC 4151 (Beckmann et al. 2005), six AGN near the Galactic plane (Soldi et al. 2005), and an early study of all extragalactic sources seen through the Galactic plane (Bassani et al. 2004). Two of the new sources discovered by *INTEGRAL*, IGR J18027-1455 and IGR J21247+5058, have also been shown to be AGN (Masetti et al. 2004).

With the on-going observation of the sky by *INTEGRAL*, a sufficient amount of data is now accessible to compile the first *INTEGRAL* catalog of AGN. In this paper we present analysis of recent observations performed by the *INTEGRAL* satellite instruments IBIS/ISGRI, SPI, and JEM-X, and compare the results with previous studies.

2. Observations

Observations in the X-ray to soft gamma-ray domain have been performed by the instruments on-board the *INTEGRAL* satellite (Winkler et al. 2003). This mission offers the unique possibility to perform simultaneous observations over the $2-8000$ keV energy region. This is achieved by the X-ray monitor (2–30 keV) JEM-X (Lund et al. 2003), the soft gamma-ray imager (20–1000 keV) ISGRI (Lebrun et al. 2003), and the spectrograph SPI (Vedrenne et al. 2003), which operates in the $20-8000$ keV region. Each of these instruments employs the coded-aperture technique (Caroli et al. 1987). In addition to these data an optical monitor (OMC, Mas-Hesse et al. 2003) provides photometric measurements in the V band.

2.1. *INTEGRAL* Data

Data used for the analysis presented here were all in the public domain by the end of March 2005. This includes data from orbit revolutions 19 - 137 and revolutions 142 - 149. Data before revolution 19 have been excluded as the instruments settings changed frequently and therefore the data from this period are not suitable to be included into a homogeneous survey. Most of the *INTEGRAL* observing time has been spent on the Galactic Plane so far, with some deep exposures at high Galactic latitude, for example in the Virgo and the Centaurus region.

Our sample objects have been selected in three ways. The first criterion was a detection in the ISGRI data in a single pointed observation. The duration of one pointing of the spacecraft is usually 2 - 3 ks long. The standard analysis of the data is performed at the *INTEGRAL* Science Data Centre (ISDC; Courvoisier et al. 2003b). These results are publicly available[1]. Within one pointing the detection threshold for a source in the center of the field of view of ISGRI is about 20 mCrab. A second level search was done using combined data sets of individual observations and contained within separate revolutions which are about 3 days long. In cases where an observation lasted longer than a revolution, the data set was split by revolution. The results from this analysis are publicly available through the HEASARC archive[2]. Clearly the sensitivity of this second method depends strongly on the duration of the analyzed observation. The sensitivity also depends on the dither pattern of the observation and on the position of the source within the field of view. In addition to those two ways of combining the list of AGN seen by *INTEGRAL*, we added all AGN which have been reported as *INTEGRAL* detections so far in the literature. This combined list of objects is presented in Table 1. In order to get meaningful results for each of the sources in this AGN sample, it was necessary to perform an individual analysis for each one. We used the data for which the spacecraft was pointed within 10 degrees radius about each AGN for ISGRI and SPI, and within 5 degrees for JEM-X. The exposure times listed in Tab. 1 refer to the effective ISGRI values. These values are approximately the same for the spectrograph SPI, but for the JEM-X monitor it has to be taken into account that they cover a much smaller sky area. Thus in the case of dithering observation, the source is not always in the field of view of the monitors, and the exposure times are correspondingly shorter.

The analysis was performed using the Offline Science Analysis (OSA) software version 5.0 distributed by the ISDC (Courvoisier et al. 2003b). This version shows substantial improvement compared to the previous OSA 4.2 version, except for the JEM-X spectral extraction, for which we used the March 15, 2005 version of the OSA. The significances listed in Tab. 1 have been derived by using the OSA software for ISGRI ($20-40$ keV), SPI ($20-40$ keV), and JEM-X ($2-20$ keV). In cases where there were no publicly available data covering the source position, we put “n/a” in the significance column. In those cases where no JEM-X or SPI detection was achieved, “–” is written. For comparison we list the photon flux measured by *CGRO*/OSSE in the $15-150$ keV energy band, as reported by Johnson et al. (1997) for Seyfert galaxies and by McNaron-Brown et al. (1995) for blazars. Apart from Gamma-ray bursts, no extragalactic source detections by IBIS/PICsIT have been reported.

The analysis of the *INTEGRAL*/IBIS data is based on a cross-correlation procedure between the recorded image on the detector plane and a decoding array derived from the mask pattern (Goldwurm et al. 2003). The ISGRI spectra have been extracted from the count rate and variance mosaic images at the position of the source, which in all cases corresponds to the brightest pixel in the $20-40$ keV band. The SPI analysis was done using the specific analysis software (Diehl et al. 2003) including version 9.2 of the reconstruction software SPIROS (Skinner & Connell 2003) which is based on the "Iterative Removal of Sources" technique (IROS; Hammersley et al. 1992): a simple image of the field of view is made using a mapping technique which is optimized for finding a source assuming that the data can be explained by only that source plus background. The mapping gives the approximate location and intensity of the source, which are then improved by maximizing a measure of the goodness of fit. The residuals of the fit are used as the input for a further image reconstruction and source search (Skinner & Connell 2003). The fitting process is easier when an input catalog is provided. In this work we used the source positions found with ISGRI as an input catalog for the SPI analysis, as the sensitivity of ISGRI is higher than that of SPI below 200 keV.

---

[1] `http://isdc.unige.ch/index.cgi?Data+sources`

[2] `http://heasarc.gsfc.nasa.gov/docs/integral/inthp_archive.html`

With respect to the calibration uncertainty, the IBIS instrument team stated that the systematic error is of the order of 1.5% (2005, private communication). Nevertheless, this value corresponds to on-axis observations within a short period of time with no disturbing influence, such as enhanced background activity. A combined fit of Crab spectra taken in revolution 43, 44, 120, 170, and 239, i.e. over a 1.5 year span of the mission, shows a larger uncertainty in the flux. The scale of diversity, assuming that Crab is a source with constant flux, gives some hint what is the scale of discrepancies in count rates observed in various conditions, i.e., with different dithering patterns or instrumental settings. Clearly the absolute calibration cannot be more precise than the observed variations. Hence, it seems that for the 22-120 keV band we may conclude that the joint 1σ uncertainty of the spectral extraction method and the calibration files is about 5%. It may happen that for other sources and in some special circumstances we may encounter a larger discrepancy especially for faint sources, but a systematic error of 5% should be a valid approximation. In most cases the fit to the data from the three instruments used in this work did not show any improvement when adding variable cross-calibration. This is mainly due to the fact that most spectra have low signal-to-noise and adding a further parameter to the fit procedure worsens the fit result, according to an F-test.

The spectral shape calibration was also tested on *INTEGRAL* Crab observations. With the so-called canonical model for the Crab showing a single power law with photon index $\Gamma = 2.1$ (Toor & Seward 1974), the values retrieved from *INTEGRAL* are $\Gamma = 2.1$ (JEM-X), and $\Gamma = 2.2$ for SPI and ISGRI (Kirsch et al. 2005). It should be kept in mind though that the Crab is significantly brighter than the sources discussed here, and systematic effects might depend on source brightness.

All the extracted images and source results are available in electronic form[3].

2.2. *CGRO* Data

CGRO/OSSE (Johnson et al. 1993) covered the energy range $50 - 10,000$ keV. It therefore preferentially detected AGN with hard and bright X-ray spectra, which we also expect to be detectable by *INTEGRAL*. Several of the AGN detected by OSSE have not been seen by *INTEGRAL* so far. We list those sources and the *INTEGRAL*/ISGRI exposure time on the particular AGN in Table 2[3].

3. X-ray to Gamma-ray Spectra

3.1. Time Averaged Spectral Analysis

The overall spectra extracted from the *INTEGRAL* JEM-X, ISGRI and SPI data for 10 AGNs are shown in Fig. 1 to Fig. 10 (see Sect. 4 for details). A single powerlaw fit with absorption from material in the line of sight has been applied to the *INTEGRAL* spectra of all sources and the results are presented in Table 3 and in Figure 11. The errors on the photon indices are 90% confidence errors. The intrinsic absorption was determined by subtracting the Galactic hydrogen column density from the total absorption as measured in the soft X-rays. In the cases where the *INTEGRAL*/JEM-

---

[3] http://heasarc.gsfc.nasa.gov/docs/integral/inthp_archive.html

X data were not available or did not restrict the absorption column density sufficiently, values from the literature have been used to fix this component in the spectral fit (Tab. 3). No systematic error has been added to the data. The spectral fitting was done using version 11.3.2 of XSPEC (Arnaud 1996). In most cases a single powerlaw gave an acceptable fit to the data, which also is based on the fact that the signal-to-noise of many of the spectral data is rather low. In six cases a cut-off power law fit led to better fits results. We report those results in Table 4.

3.2. Averaged Spectra of AGN Subtypes

In order to investigate the spectra of AGN subtypes, we have derived averaged spectra of the Seyfert 1 and 2 types, as well as for the intermediate Seyferts and the blazars, and according to the intrinsic absorption. The average Seyfert 1 spectrum was constructed using the weighted mean of 10 ISGRI spectra, the Seyfert 2 composite spectrum includes 15 sources, and 8 objects form the intermediate Seyfert 1.5 group. The two brightest sources, Cen A and NGC 4151, have been excluded from the analysis as their high signal-to-noise ratio would dominate the averaged spectra. The average spectra have been constructed by computing the weighted mean of all fit results on the individual sources as shown in Table 3. In order to do so, all spectra had been fit by an absorbed single powerlaw model. When computing the weighted average of the various sub classes, the Seyfert 2 objects show flatter hard X-ray spectra ($\Gamma = 1.95 \pm 0.01$) than the Seyfert 1.5 ($\Gamma = 2.10 \pm 0.02$), and Seyfert 1 appear to have the steepest spectra ($\Gamma = 2.11 \pm 0.05$) together with the blazars ($\Gamma = 2.07 \pm 0.10$).

The classification according to the Seyfert type of the objects is based on optical observations. An approach to classify sources due to their properties in the X-rays can be done by separating the sources with high intrinsic absorption ($N_{\rm H} > 10^{22}\,{\rm cm^{-2}}$) from those objects which do not show significant absorption in the soft X-rays. It has to be pointed out that not all objects which show high intrinsic absorption in the X-rays are classified as Seyfert 2 galaxies in the optical, and the same applies for the other AGN sub-types. Nevertheless a similar trend in the spectral slopes can be seen: the 21 absorbed AGN show a flatter hard X-ray spectrum ($\Gamma = 1.98 \pm 0.01$) than the 13 unabsorbed sources ($\Gamma = 2.08 \pm 0.02$). The blazars have again been excluded from these samples.

4. Notes on Individual Sources

Spectra are presented in this paper for *INTEGRAL* sources which are as yet not published and for which at least two instruments yield a detection of $> 3\sigma$. Spectral fits did not require any cross-calibration correction between the instruments, except for GRS 1734-292 and for the two brightest sources, Cen A and NGC 4151. In cases where the spectra of different instruments overlap, the spectral plots have been performed in count space, otherwise in photon space.

NGC 1275, a Seyfert 2 galaxy at $z = 0.018$, was detected in the ISGRI and JEM-X data (Fig. 1). The spectrum represents the blend of the Perseus cluster with the spectrum of the AGN. The measured spectrum in the $2 - 400\,{\rm keV}$ energy range is fitted by a slightly absorbed ($N_{\rm H} = (6.7^{+8.1}_{-6.7}) \times 10^{21}\,{\rm cm^{-2}}$) bremsstrahlung model ($kT = 3.4^{+0.4}_{-0.4}$) plus a powerlaw with a photon index fixed to the measurement from the ISGRI data ($\Gamma = 2.12$). In addition a Gaussian line with $E = 6.9^{+0.2}_{-0.2}\,{\rm keV}$ and an equivalent width of $EW = 670\,{\rm eV}$ has been applied to achieve a reasonable fit result ($\chi^2_\nu = 0.98$). We see no evidence of flattening of the continuum above $\sim 10\,{\rm keV}$, which is often attributed to Compton reflection, nor can we quantitatively identify a spectral break.

NGC 4507 (Seyfert 2; $z = 0.012$) was detected by ISGRI and SPI (Fig. 2). The combined data are best represented by a power-law ($\Gamma = 1.0^{+1.7}_{-0.8}$) with a high energy cut-off ($E_{\rm cut} = 55^{+123}_{-11}\,{\rm keV}$). This is consistent with results from *Ginga* and OSSE, which showed $\Gamma = 1.3 \pm 0.2$ and $E_{\rm cut} = 73^{+48}_{-24}\,{\rm keV}$ (Bassani et al. 1995).

NGC 4593, a Seyfert 1 galaxy in the Virgo region at $z = 0.009$, shows a cut-off powerlaw with $\Gamma = 1.0^{+0.6}_{-0.6}$ and $E_{\rm cut} = 35^{+49}_{-12}\,{\rm keV}$ and is detected up to 150 keV (Fig. 3) with a flux of $f_{20-100\,{\rm keV}} = 6.8 \times 10^{-11}{\rm erg\,cm^{-2}\,s^{-1}}$ ($\chi^2_\nu = 1.00$). This is significantly different from the spectrum measured by *BeppoSAX* : $\Gamma = 1.94^{+0.06}_{-0.05}$ and $E_{\rm cut} \gg 222\,{\rm keV}$ (Guainazzi et al. 1999) with a similar flux ($f_{20-100\,{\rm keV}} = 7 \times 10^{-11}{\rm erg\,cm^{-2}\,s^{-1}}$).

Cen A, a Seyfert 2 ($z = 0.0018$) is one of the brightest objects in the sample. The statistics al-low in this case to determine the intercalibration factors between JEM-X, ISGRI, and SPI (1.0 : $0.92^{+0.04}_{-0.04}$: $1.10^{+0.06}_{-0.06}$). An absorbed power law plus a Gaussian line gives the best fit to the data with $N_H = 14.6^{+1.4}_{-1.4} \times 10^{22}\,\mathrm{cm^{-2}}$, $\Gamma = 1.96^{+0.02}_{-0.02}$, and an equivalent width of the iron Kα line of $EW = 108\,\mathrm{eV}$. Adding an exponential cut-off does not improve the fit ($E_C = 870^{+3810}_{-410}\,\mathrm{keV}$). The results are consistent with results published on a subset of *INTEGRAL* data and with *BeppoSAX* data (Soldi et al. 2005).

MCG –06–30–015: The Seyfert 1 galaxy ($z = 0.0077$) was detected by all three instruments (Fig. 4). The spectrum is well represented ($\chi^2_\nu = 1.19$) by a power law with $\Gamma = 2.8^{+0.4}_{-0.3}$ and weak evidence for absorption of $N_\mathrm{H} = 5.9^{+8.6}_{-5.5} \times 10^{22}\,\mathrm{cm^{-2}}$ ($\chi^2_\nu = 1.11$).

4U 1344–60 is a bright ($f_{20-100\,\mathrm{keV}} = 5.7 \times 10^{-11}\mathrm{erg\,cm^{-2}\,s^{-1}}$) X-ray source, which has been unidentified until Michel et al. (2004) reported the identification of this source as a low redshift AGN but no further information was provided. In order to clarify the nature of this object, we analyzed 31 ks of XMM-Newton data of the Centaurus B field, taken in August 2001. Although 4U 1344–60 appears to be near to the rim of the EPIC camera, a spectrum can be extracted from EPIC/pn data which shows an iron line at $6.13^{+0.08}_{-0.09}\,\mathrm{keV}$ with a flux of $f_{K\alpha} = 1.8^{+0.2}_{-0.3} \times 10^{-4}\,\mathrm{ph\,cm^{-2}\,s^{-1}}$ and an equivalent width of 410 eV. If we consider this line to be the iron Kα fluorescence line at 6.4 keV, the redshift of 4U 1344–60 is $z = 0.043^{+0.016}_{-0.014}$. The simultaneous fit with the *INTEGRAL* ISGRI and SPI data shows that the spectrum is well represented by an absorbed power law plus Gaussian line with $N_\mathrm{H} = 2.64^{+0.07}_{-0.07} \times 10^{22}\,\mathrm{cm^{-2}}$ and $\Gamma = 1.65^{+0.02}_{-0.03}$ ($\chi^2_\nu = 1.06$ for 711 dof; Fig. 5).

IC 4329A (Seyfert 1.2; $z = 0.016$) is well represented by a powerlaw ($\Gamma = 1.5^{+0.4}_{-0.4}$) with exponential cut-off ($E_C = 104^{+344}_{-48}\,\mathrm{keV}$), see Fig. 6. The results are consistent on a $2-3\sigma$ level with the spectrum measured by *BeppoSAX* ($\Gamma = 1.90 \pm 0.05$, $E_C \simeq 300\,\mathrm{keV}$; Perola et al. 2002).

NGC 5506: The JEM-X and ISGRI spectrum of this Seyfert 1.9 ($z = 0.006$) shows an absorbed ($N_\mathrm{H} = 2.7^{+2.4}_{-2.3} \times 10^{22}\,\mathrm{cm^{-2}}$) high-energy cut-off spectrum with $\Gamma = 1.81^{+0.25}_{-0.28}$ and $E_\mathrm{cut} = 57^{+139}_{-27}$ keV ($\chi^2_\nu = 1.07$; Fig. 7). No SPI data are available for this source, because SPI was undergoing an annealing cycle during the observations of NGC 5506. The results are consistent with *BeppoSAX* measurements (Bianchi et al. 2003), even though the iron Kα line and the reflection component are not detectable in the *INTEGRAL* data.

IC 4518 (VV 780): This Seyfert 2 galaxy ($z = 0.016$) was reported to be detectable in a 700 ks observation in January 2004 on SN 1006 (Kalemci et al. 2005). The source was detected with 8.7σ in the $20-40\,\mathrm{keV}$ band with a photon index of $\Gamma = 2.2 \pm 0.4$ and a flux of $f_{20-40\,\mathrm{keV}} = 6.8 \times 10^{-12}\mathrm{erg\,cm^{-2}\,s^{-1}}$. Note that in Tab. 1 and Tab. 3 we refer to our measurements, which are consistent with the values derived by Kalemci et al. 2005.

GRS 1734–292 (AX J1737.4–2907): This Seyfert 1 galaxy ($z = 0.021$) is located near to the Galactic Center ($l = 358.9°$, $b = 1.4°$). Because this region is monitored regularly by *INTEGRAL*, 3.3 Msec of observations are available in the public data. Even though an ISGRI spectrum of this source has been published already (Sazonov et al. 2004), we discuss this object in more detail, because Sazonov et al. included neither the JEM-X, nor the SPI data in their study. The fact that the source is located in a crowded region, makes the analysis more difficult, especially for SPI data with its $\sim 2.5°$ spatial resolution. Figure 8 shows the combined JEM-X2, ISGRI, and SPI spectrum. The data are represented by a simple powerlaw with $\Gamma = 2.63^{+0.09}_{-0.09}$ and in this case intercalibration factors had to be applied to achieve an acceptable fit result ($\chi^2_\nu = 1.09$, 161 d.o.f.). Adding a cut-off or an absorption component to the model does not improve the fit. The average flux is $f_{20-40\,\mathrm{keV}} = 9 \times 10^{-11}\mathrm{erg\,cm^{-2}\,s^{-1}}$. This source is of additional interest, as it lies within the error circle for the EGRET source 3EG J1736-2908 (Sazonov et al. 2004). If this is a real association it would be the only known case of a “gamma-ray loud” Seyfert 1.

MRK 509 (Seyfert 1; $z = 0.034$) was not detected by SPI and yielded only low signal-to-noise spectra with JEM-X and ISGRI (Fig. 9). No absorption component was necessary to fit the combined spectrum. A pure single powerlaw ($\Gamma = 1.66^{+0.15}_{-0.16}$) resulted in $\chi^2_\nu = 0.99$, consistent with measurements by *XMM-Newton* ($\Gamma = 1.75$; Pounds et al. 2001) and with *Bep-*

poSAX ($\Gamma = 1.58^{+0.09}_{-0.08}$), although the latter data showed in addition a cut-off at $E_C = 67^{+30}_{-20}$ keV (Perola et al. 2002).

S5 0716+714: Results on *INTEGRAL* observations of this BL Lac object have been published by Pian et al. 2005. Using the OSA reduction version 4.0 they achieved a marginal detection of 4.5σ in the $30-60$ keV band. Using more data and the current version of the software the source is not detectable, but the strong variability of the source might have resulted in a low average flux.

3C 279: This blazar ($z = 0.5362$) led to a weak detection with JEM-X and to none with SPI. The spectrum, model shown in Fig. 10, is dominated by the ISGRI statistics and is well represented by a single powerlaw with photon index $\Gamma = 1.3^{+0.7}_{-0.5}$ ($\chi^2_\nu = 0.98$), consistent with *BeppoSAX* ($\Gamma = 1.66 \pm 0.05$, Ballo et al. 2002) and *CGRO*/OSSE observations ($\Gamma = 2.1^{+0.4}_{-0.4}$; McNaron-Brown et al. 1995). The JEM-X data show an excess in the $2-7$ keV energy band. This excess might be caused by the transition from the synchrotron to the inverse Compton branch in this energy range, which would lead to a convex spectrum.

Several sources may have been marginally suspected in the *INTEGRAL* data. They were either targets of dedicated observations or were detected in some single science windows. We performed the same analysis as for the other sources presented here, but found only spurious source candidates which result from image reconstruction problems like ghosts, mask patterns, etc. Among those sources are **MRK 231**, **ESO 33–2**, **PKS 0637–75**, **MCG –05–23–16**, **QSO 1028+313**, **NGC 4736**, **NGC 4418**, **3C 353**, and **QSO 1730–130**[3].

5. Distribution in Space and Sample Completeness

In order to explore the space distribution of hard X-ray selected objects, one generally needs to consider a statistically complete flux-limited sample. However, this is difficult to achieve with a data set comprised of various lines of sight and widely differing exposures. In addition, the telescope effective area can be highly position dependent within the coded aperture field of view. Thus, we opt to leave the compilation of a log-N log-S distribution, and perhaps a hard X-ray AGN luminosity distribution to a future paper.

Alternatively, the V_e/V_a-test is a simple method developed by Avni & Bahcall (1980) based on the V/V_{max} test of Schmidt (1968). V_e stands for the volume, which is enclosed by the object, and V_a is the accessible volume, in which the object could have been found (e.g. due to a flux limit of a survey). Avni & Bahcall showed that different survey areas with different flux limits in various energy bands can be combined by the V_e/V_a-test. In the case of no evolution $\langle V_e/V_a \rangle = 0.5$ is expected and the error $\sigma_m(n)$ for a given mean value $\langle m \rangle = \langle V_e/V_a \rangle$ based on n objects is

$$\sigma_m(n) = \sqrt{\frac{1/3 - \langle m \rangle + \langle m \rangle^2}{n}} \qquad (1)$$

This evolutionary test is applicable only to samples with a well-defined flux limit down to which all objects have been found. It can therefore also be used to test the completeness of a sample. We performed a series of V_e/V_a-tests to the *INTEGRAL* AGN sample, assuming completeness limits in the range of 1σ up to 15σ ISGRI $20-40$ keV significance, adding 5% systematic error to the flux uncertainty as described in Section 2.1. For a significance limit below the true completeness limit of the sample one expects the V_e/V_a-tests to derive a value $\langle V_e/V_a \rangle < \langle V_e/V_a \rangle_{true}$, where $\langle V_e/V_a \rangle_{true}$ is the true test result for a complete sample. Above the completeness limit the $\langle V_e/V_a \rangle$ values should be distributed around $\langle V_e/V_a \rangle_{true}$ within the statistical uncertainties. The results of the tests are shown in Figure 12. It appears that the sample becomes complete at a significance level around $> 6\sigma$, including 31 AGN. The average value above this significance is $\langle V_e/V_a \rangle = 0.505 \pm 0.022$. This value is consistent with the expected value of 0.5 which reflects no evolution and an even distribution in the local universe. If we do not apply the 5% systematic error to the data, the average value is lower ($\langle V_e/V_a \rangle = 0.428 \pm 0.018$), indicating that a systematic error is indeed apparent in the ISGRI data.

6. Discussion

The typical *INTEGRAL* spectrum can be described by a simple powerlaw model with average photon indices ranging from $\Gamma = 2.0$ for obscured AGN to $\Gamma = 2.1$ for unabsorbed sources

(Tab. 5). The simple model does not give reasonable results in cases of high signal-to-noise, where an appropriate fit requires additional features such as a cut-off and a reflection component (Soldi et al. 2005; Beckmann et al. 2005). The results presented here show slightly steeper spectra than previous investigations of AGN in comparable energy ranges. The same trend is seen in the comparison of Crab observations, where the *INTEGRAL*/ISGRI spectra also appear to be slightly steeper than in previous observations (Kirsch et al. 2005), and in comparison of *RXTE* and *INTEGRAL*/ISGRI spectra of Cen A (Rothschild et al. 2006).

Zdziarski et al. (1995) did a study of Seyfert galaxies observed by *Ginga* and *CGRO*/OSSE, with a similar redshift distribution ($\bar{z} = 0.022$) as the Seyferts detected by *INTEGRAL* ($\bar{z} = 0.020$). The same trend in spectral slope from $\Gamma = 1.92\,^{+0.03}_{-0.03}$ for radio-quiet Seyfert 1 down to $\Gamma = 1.67\,^{+0.31}_{-0.49}$ for Seyfert 2 was detectable in the sample, and a potential cut-off appeared at energies $E_C > 250\,\mathrm{keV}$. The average of all Seyfert spectra ($\Gamma = 1.9$) appears to be similar to the one in our sample ($\Gamma = 1.96 \pm 0.01$).

Gondek et al. (1996) confirmed that Seyfert 1 galaxies show a continuum with photon index $\Gamma = 1.9^{+0.1}_{-0.1}$ with high energy cut-off $E_C > 500\,\mathrm{keV}$ and moderate reflection component ($R = 0.76\,^{+0.15}_{-0.15}$), based on *EXOSAT*, *Ginga*, *HEAO-1*, and *CGRO*/OSSE data. More recent studies by Perola et al. (2002) on *BeppoSAX* data of 9 Seyfert 1 galaxies confirmed this picture. Malizia et al. (2003) used the *BeppoSAX* data (3 – 200 keV) of 14 Seyfert 1 and 17 Seyfert 2 to study average spectral properties. Also this work finds Seyfert 1 galaxies to be softer ($\Gamma \sim 1.9$) than Seyfert 2 ($\Gamma \sim 1.75$), which also show stronger absorption. Both types show iron lines with an equivalent width of 120 eV and a Compton reflection component of $R \sim 0.6 - 1$, but the energy cut-off of the type 1 objects appears to be at higher energies (200 keV compared to $E_C \sim 130\,\mathrm{keV}$ for the Seyfert 2).

Deluit & Courvoisier (2003) used for their analysis only the *BeppoSAX*/PDS spectra of 14 Seyfert 1, 9 Seyfert 1.5, and 22 Seyfert 2. This study lead to a somewhat different result. Contrary to other studies Seyfert 2 objects show a steeper spectrum ($\Gamma = 2.00\,^{+0.05}_{-045}$) than Seyfert 1 ($\Gamma = 1.89\,^{+0.28}_{-0.46}$), but with the large error on the results, the difference is not significant. A cut-off does not seem to be required by the *BeppoSAX* data. A marginally significant cut-off is detected in the Seyfert 1 spectra with $E_C = 221\,^{+\infty}_{-158}\,\mathrm{keV}$. The average spectra show moderate reflection for Seyfert 1/2 objects ($R = 0.48$ and $R = 0.39$, respectively), while the Seyfert 1.5 appear to have $R = 2.33$ (Deluit & Courvoisier 2003). It has to be kept in mind that the results in this study are based on *BeppoSAX*/PDS spectra alone, without taking into account the valuable information from the lower energy LECS/MECS data, which could have significantly constrained the shape of the underlying continuum.

The *INTEGRAL* AGN sample confirms the previously found trend with harder spectra for the obscured objects. This can be roughly understood by the argument that in order to overcome a substantial absorption, obscured objects have to have hard X-ray spectra to be detectable. Comparing the ratio X of obscured ($N_\mathrm{H} > 10^{22}\,\mathrm{cm}^{-2}$) to unobscured AGN we find in the *INTEGRAL* data that $X = 1.7 \pm 0.4$. Excluding the targets of observations, leads to $X = 1.6 \pm 0.5$. The ratios change slightly when taking into account only those objects which belong to the complete sample with an ISGRI significance of 7σ or higher (Tab. 1). This sub-sample includes 32 AGN, with 18 obscured and 10 unobscured objects (absorption information is missing for the remaining four objects). Using only the complete sample changes the ratio to $X = 1.8 \pm 0.5$ and $X = 1.9 \pm 0.6$ (targets excluded), respectively. Splitting this result up into objects near the Galactic plane ($|b| < 20^\circ$) and off the plane shows for all objects a ratio of $X = 3.3 \pm 1.1$ and $X = 1.1 \pm 0.5$, respectively. This trend shows that the harder spectra of those objects, where the absorption in the line of sight through the Galaxy is low compared to the intrinsic absorption, are more likely to shine through the Galactic plane.

One would expect a higher ratio in order to explain the unresolved X-ray background in this energy range (e.g. Worsley et al. 2005). But it has to be taken into account that our sample only represents the high flux and low luminosity sources ($\langle \log L_X \rangle = 43.3$) in the local universe ($\langle z \rangle = 0.020$). Gilli et al. (1999) showed that the ratio between type 2 and all QSOs should be at most 2 in the local universe. The *BeppoSAX* HELLAS survey showed that the fraction of unobscured AGN increases with the flux of the objects (Comastri et al. 2001). Evidence that the fraction of obscured AGN depends on the redshift was found by Ueda et al. (2004) when studying the hard X-ray luminosity function. They find that the density evolution of AGN depends on the luminosity which will lead to an increase of the type 2 fraction with redshift. In a recent study La Franca et al. (2005) find that both effects combined (the fraction of absorbed AGN decreases with the intrinsic X-ray luminosity, and increases with the redshift) can be explained by a luminosity-dependent density evolution model. They further show that the luminosity function of AGN, like those presented here, peaks at $z \sim 0.7$ while high luminosity AGN peak at $z \sim 2$. Consistent with our study, La Franca et al. also find a ratio of $X = 2.1$ at $L_X = 10^{42.5}\,\mathrm{erg\,s^{-1}}$ in the $2-10\,\mathrm{keV}$ energy band. Unified models predict, depending on the applied model, a ratio of $X = 1.5-2.0$ for high flux low redshift AGN (Treister & Urry 2005), while a recent study of *Chandra* data showed that $X = 8.5 \pm 6.3$ for low redshift, low luminosity AGN (Barger et al. 2005), indicating a larger dominance of obscured objects. These investigations have been focused so far on the X-rays below 10 keV, and *INTEGRAL* can add substantial information to the nature of bright AGNs in the local universe. Considering the expected composition of the hard X-ray background, it is remarkable that our sample includes only 4 Compton thick AGN. If Compton thick AGN are dominant in the hard X-rays, they would have to be fainter than the objects detected by *INTEGRAL* so far.

The energy range in the $15-200\,\mathrm{keV}$ is now also accessible through the BAT instrument aboard *Swift* (Gehrels et al. 2005). A study by Markwardt et al. (2005) of observations of the extragalactic sky indicates a ratio of $X = 2$ between obscured and unobscured AGN, fully consistent with the results from the *INTEGRAL* AGN sample. Although the *Swift*/BAT survey covers different areas of the sky, the energy band is similar to the *INTEGRAL*/ISGRI range and the type of AGNs detectable should be the same.

The sample presented here is still too small to constrain the ratio of obscured to unobscured sources, but it might indicate that the unified model predicts this value of $X \simeq 2$ correctly, differing from earlier claims (Treister & Urry 2005; La Franca et al. 2005).

7. Conclusions

The AGN sample derived from the *INTEGRAL* public data archive comprises 42 low luminosity and low redshift ($\langle \log L_X \rangle = 43.3$, $\langle z \rangle = 0.020 \pm 0.004$, excluding the blazars) objects including 5 blazars in the hard X-ray domain. Only one galaxy cluster is also detected, but no starburst galaxy has been as yet. The results from the JEM-X2, ISGRI, and SPI data show that within the statistical limitations of the data the high-energy continua of AGN can be described by a simple powerlaw with photon index $\Gamma = 2.11 \pm 0.05$ (Seyfert 1), $\Gamma = 2.10 \pm 0.02$ (Seyfert 1.5), and $\Gamma = 1.95 \pm 0.01$ (Seyfert 2). A similar trend is seen when dividing the Seyfert galaxies according to their intrinsic absorption into unabsorbed ($N_H < 10^{22}\,\mathrm{cm^{-2}}$; $\Gamma = 2.08 \pm 0.02$) and absorbed sources ($\Gamma = 1.98 \pm 0.01$). Blazars naturally show strongly variable spectra, but the average spectral slope is of the same order ($\Gamma = 2.07 \pm 0.10$). It has to be taken into account that the simple model does not represent the data as soon as a sufficient signal-to-noise is apparent, like in the Circinus galaxy and Cen A (Soldi et al. 2005; Rothschild et al. 2006) or NGC 4151 (Beckmann et al. 2005). But the average spectra indicate that a cut-off in most cases, if apparent, appears at energies $E_C \gg 200\,\mathrm{keV}$.

The AGN sample presented here is complete down to a significance limit of $\sim 7\sigma$. This results in a complete sample of 32 AGN. Within this complete sample the ratio between obscured and unobscured AGN is $X = 1.8 \pm 0.5$, consistent with the unified model for AGN and with recent results from the *Swift*/BAT survey. Only 4 Compton thick AGN are found in the whole and only 3 in the complete sample.

Sazonov et al. (2005) report five additional AGN in recent observations, not detectable in the data presented here. Additionally one AGN seen by OSSE, the blazar 3C 454.3 (McNaron-Brown et al. 1995), has recently been detected by *INTEGRAL* during an outburst (Foschini et al. 2005). With the ongoing observations of the *INTEGRAL* and *Swift* mission, the number of detectable AGNs will increase further, especially with a number of already performed and scheduled observations far off the Galactic plane. This will enable us to solve the mystery of the hard X-ray background above 10 keV in the near future.

We like to thank the anonymous referee for the comments which helped to improve the paper. This research has made use of the NASA/IPAC Extragalactic Database (NED) which is operated by the Jet Propulsion Laboratory, of data obtained from the High Energy Astrophysics Science Archive Research Center (HEASARC), provided by NASA's Goddard Space Flight Center, and of the SIMBAD Astronomical Database which is operated by the Centre de Données astronomiques de Strasbourg. This research has made use of the Tartarus (Version 3.1) database, created by Paul O'Neill and Kirpal Nandra at Imperial College London, and Jane Turner at NASA/GSFC. Tartarus is supported by funding from PPARC, and NASA grants NAG5-7385 and NAG5-7067.

REFERENCES

Arnaud, K.A. 1996, in: Astronomical Data Analysis Software and Systems V, eds. Jacoby G. and Barnes J., p17, ASP Conf. Series 101

Avni, Y. & Bahcall, J. N. 1980, ApJ, 235, 694

Ballo, L., et al. 2002, ApJ, 567, 50

Barger, A. J., Cowie, L. L., Mushotzky, R. F., Yang, Y., Wang, W.-H., Steffen, A. T., & Capa, P. 2005, AJ, 129, 578

Bassani, L., Malagutti, G., Jourdain, E., Roques, J. P., Johnson, W. N. 1995, ApJ, 444, L73

Bassani, L., et al. 2004, in: Proc. 5th INTEGRAL Workshop, ESA SP-552, 139, astro-ph/0404442

Beckmann, V., Gehrels, N., Favre, P., Walter, R., Courvoisier, T. J.-L., Petrucci, P.-O., Malzac, J. 2004, ApJ, 614, 641

Beckmann, V. et al. 2005, ApJ accepted, astro-ph/0508327

Bianchi, S., Balestra, I., Matt, G., Guainazzi, M., Perola, G. C. 2003, A&A, 402, 141

Boella, G., Butler, R. C., Perola, G.C., Piro, L., Scarsi, L., Bleeker, J. A. M. 1997, A&AS, 122, 299

Brandt, W. N., & Hasinger, G. 2005, ARA&A, 43

Caroli, E., Stephen, J. B., Di Cocco, G., Natalucci, L., Spizzichino, A. 1987, Space Sci. Rev., 45, 349

Comastri, A., Setti, G., Zamorani, G., Hasinger, G. 1995, A&A, 296, 1

Comastri, A., Fiore, F., Vignali, C., Matt, G., Perola, G. C., & La Franca, F. 2001, MNRAS, 327, 781

Courvoisier, T.J.-L., Beckmann, V., Bourban, G., et al. 2003a, A&A, 411, L343

Courvoisier, T.J.-L., Walter, R., Beckmann, V., et al. 2003b, A&A, 411, L53

Deluit, S., & Courvoisier, T. J.-L. 2003, A&A, 399, 77

De Rosa, A., et al. 2005, A&A, 438, 121

Diehl, R., Baby, N., Beckmann, V., et al. 2003, A&A, 411, L117

Foschini, L., et al. 2005, ATEL, 497

Fossati, G., Maraschi, L., Celotti, A., Comastri, A., & Ghisellini, G. 1999, MNRAS, 299, 433

Frontera, F., Costa, E., & Dal Fiume, D. 1997, A&AS, 122, 357

Gehrels, N., et al. 2005, ApJ, 611, 1005

Gehrels, N., Chipman, E., & Kniffen, D. A. 1993, A&AS, 97, 5

George, I. M., & Fabian, A. C. 1991, MNRAS, 249, 352

Gilli, R., Salvati, M., Hasinger, G., 2001, A&A, 366, 407

Gilli, R., Risaliti, G., & Salvati, M. 1999, A&A, 347, 424

Goldwurm, A., et al. 2003, A&A, 411, L223

Gondek, D., et al. 1996, MNRAS, 282, 646

Guainazzi, M., et al. 1999, A&A, 346, 407

Hammersley, A. P., Ponman, T. J., & Skinner, G. K. 1992, NIMS, A311, 585

Johnson, W. N., et al. 1993, ApJS, 86, 693

Johnson, W. N., Zdziarski, A. A., Madejski, G. M., Paciesas, W. S., Steinle, H., & Lin, Y.-C. 1997, in The Fourth Compton Symposium, C. D. Dermer et al. (eds.) New York: AIP, p. 283

Kalemci, E., Boggs, S. E., Lund, N. 2005, ATEL, 410

Kirsch, M. G., et al. 2005, in Proc. SPIE Annual Meeting, San Diego, USA, August 2005, 5898-03, astro-ph/0508235

Krivonos, R., Vikhlinin, A., Churazov, E., Lutovinov, A., Molkov, S., & Sunyaev, R. 2005, ApJ, 625, 89

La Franca, F., et al. 2005, ApJ in press, astro-ph/0509081

Lebrun, F., et al. 2003, A&A, 411, L141

Levenson, N. A., Weaver, K. A., & Heckman, T. M. 2001, ApJS, 133, 269

Lund, N., et al. 2003, A&A, 411, L231

Lutz, D., Maiolino, R., Spoon, H. W. W., Moorwood, A. F. M. 2004, A&A, 418, 465

Malizia, A., Bassani, L., Stephen, J. B., Di Cocco, G., Fiore, F., & Dean, A. J., 2003, ApJ, 589, L17

Markwardt, C. B., Tueller, J., Skinner, G. K., Gehrels, N., Barthelmy, S. D., Mushotzky, R. F. 2005, ApJL accepted, astro-ph/0509860

Mas-Hesse, J. M., et al. 2003, A&A, 411, L261

Masetti, N., Palazzi, E., Bassani, L., Malizia, A., Stephen, J. B. 2004, A&A, 426, L41

Matsumoto, C., Nava, A., Maddox, L. A., Leighly, K. M., Grupe, D., Awaki, H., Ueno, S. 2004, ApJ, 617, 930

Matt, G., et al. 1997, A&A, 325, L13

McNaron-Brown, K., et al. 1995, ApJ, 451, 575

Michel, L., Herent, O., Motch, C., Pye, J., & Watson, M.G. 2004, ASP Conf. Series, 314, 570

Paul, J., et al. 1991, Adv.Sp.Res. 11, 8, 289

Perola, G. C., et al. 2002, A&A, 389, 802

Pian, E., et al. 2005, A&A, 429, 427

Pounds, K., Reeves, J., O'Brien, P., Page, K., Turner, M., & Nayakshin, S. 2001, ApJ, 559, 181

Rothschild, R. E., et al. 2006, ApJ submitted

Sazonov, S. Y., Revnivtsev, M. G., Lutovinov, A. A., Sunyaev, R. A., & Grebenev, S. A. 2004, A&A, 421, L21

Sazonov, S. Y. & Revnivtsev, M. G. 2004, A&A, 423, 469

Sazonov, S. Y., Churazov, E., Revnivtsev, M. G., Vikhlinin, A., Sunyaev, R., 2005, A&A accepted, astro-ph/0508593

Schmidt, M., 1968, ApJ, 151, 393

Setti, G., Woltjer, L. 1989, A&A, 224, L21

Skinner, G., & Connell, P. 2003, A&A, 411, L123

Soldi, S., Beckmann, V., Bassani, L., et al. 2005, A&A accepted, astro-ph/0509123

Toor, A., & Seward, F. D. 1974, AJ, 79, 995

Treister, E., & Urry, C. M. 2005, ApJ, 630, 115

Ubertini, P. 2003, A&A, 411, L131

Vedrenne, G., et al. 2003, A&A, 411, L63

Véron-Cetty, M. P. & Véron, P. 2000, A&A Rev., 10, 81

Winkler, C., et al. 2003, A&A, 411, L1

Worsley, M. A., et al. 2005, MNRAS, 357, 1281

Young, A. J., Wilson, A. S., Terashima, Y., Arnaud, K. A., Smith, D. A. 2002, ApJ, 564, 176

Zdziarski, A. A., Johnson, W. N., Done, C., Smith, D., & McNaron-Brown, K. 1995, ApJ, 438, L63

This 2-column preprint was prepared with the AAS LATEX macros v5.2.

Table 1
INTEGRAL AGN catalog

Name	Type	z	R.A.	DEC	exp.[a] [ks]	target	ISGRI [σ]	SPI [σ]	JEM-X [σ]	OSSE[b]
NGC 788	Sy 1/2	0.0136	02 01 06	–06 46 56	311	–	10.1	–	–	–
NGC 1068	Sy 2	0.003793	02 42 41	–00 00 48	311	–	4.4	–	–	–
NGC 1275	Sy 2	0.017559	03 19 48	+41 30 42	264	–	19.1	–	78	1.8 ± 0.5
3C 111	Sy 1	0.048500	04 18 21	+38 01 36	67	–	9.5	0.1	–	2.7 ± 0.5
MCG +8–11–11	Sy 1.5	0.020484	05 54 54	+46 26 22	21	–	5.5	–	–	3.7 ± 0.3
MRK 3	Sy 2	0.013509	06 15 36	+74 02 15	472	–	13.3	2.9	–	1.8 ± 0.4
MRK 6	Sy 1.5	0.018813	06 52 12	+74 25 37	482	–	8.8	1.1	–	–
NGC 4051	Sy 1.5	0.002336	12 03 10	+44 31 53	443	–	8.8	3.0	–	–
NGC 4151	Sy 1.5	0.003320	12 10 33	+39 24 21	483	X	163.3	27.2	2089	24.5 ± 0.4
NGC 4253	Sy 1.5	0.012929	12 18 27	+29 48 46	715	–	4.3	3.1	–	–
NGC 4388	Sy 2	0.008419	12 25 47	+12 39 44	215	X	37.9	4.0	19	9.1 ± 0.4
NGC 4395	Sy 1.8	0.001064	12 25 49	+33 32 48	739	–	10.0	–	–	–
NGC 4507	Sy 2	0.011801	12 35 37	–39 54 33	152	–	15.8	3.6	n/a	5.2 ± 0.6
NGC 4593	Sy 1	0.009000	12 39 39	–05 20 39	723	–	20.9	3.8	3	< 2.9
Coma Cluster	GClstr	0.023100	12 59 48	+27 58 48	516	X	6.6	1.4	8.9	–
NGC 4945	Sy 2	0.001878	13 05 27	–49 28 06	276	X	33.4	6.7	–	10.9 ± 0.7
ESO 323–G077	Sy 2	0.015014	13 06 26	–40 24 53	761	–	9.9	1.3	–	–
NGC 5033	Sy 1.9	0.002919	13 13 28	+36 35 38	377	–	2.9	1.2	–	–
Cen A	Sy 2	0.001830	13 25 28	–43 01 09	532	X	166.1	24.8	1479	42.5 ± 0.4
MCG–06–30–015	Sy 1	0.007749	13 35 54	–34 17 43	567	X	2.9	2.2	9	4.1 ± 0.6
4U 1344–60	?	0.043	13 47 25	–60 38 36	603	–	40.9	5.9	–	–
IC 4329A	Sy 1.2	0.016054	13 49 19	–30 18 36	440	X	43.5	6.2	1	7.5 ± 0.4
Circinus gal.	Sy 2	0.001448	14 13 10	–65 20 21	589	–	79.5	8.6	2	–
NGC 5506	Sy 1.9	0.006181	14 13 15	–03 12 27	101	X	19.6	n/a	39	5.0 ± 0.6
PG 1416-129	Sy 1	0.129280	14 19 04	–13 10 44	117	–	12.0	1.1	n/a	–
IC 4518	Sy 2	0.015728	14 57 43	–43 07 54	338	–	4.8	0.5	–	–
NGC 6221	Sy 1/2	0.004977	16 52 46	–59 13 07	523	–	7.6	7.0	–	–
NGC 6300	Sy 2	0.003699	17 17 00	–62 49 14	173	–	9.8	–	3	–
GRS 1734-292	Sy 1	0.021400	17 37 24	–29 10 48	3332	–	43.8	16.9	15.2	–
IGR J18027-1455	Sy 1	0.035000	18 02 47	–14 54 55	942	–	12.1	5.8	14	–
ESO 103-G35	Sy 2	0.013286	18 38 20	–65 25 39	36	–	12.2	1.5	–	–
1H 1934-063	Sy 1	0.010587	19 37 33	–06 13 05	684	–	6.6	4.4	–	–
NGC 6814	Sy 1.5	0.005214	19 42 41	–10 19 25	488	–	13.9	1.7	–	2.8 ± 0.5
Cygnus A	Sy 2	0.056075	19 59 28	+40 44 02	1376	–	7.3	2.5	–	–
MRK 509	Sy 1	0.034397	20 44 10	–10 43 25	73	X	10.1	2.6	6	3.6 ± 0.6
IGR J21247+5058	radio gal.?	0.3[c]	21 24 39	+50 58 26	213	–	30.8	5.2	–	–
MR 2251-178	Sy 1	0.063980	22 54 06	–17 34 55	489	X	35.9	1.9	–	–
MCG -02-58-022	Sy 1.5	0.046860	23 04 44	–08 41 09	489	–	5.9	1.6	–	3.3 ± 0.8
S5 0716+714	BL Lac	0.3[c]	07 21 53	+71 20 36	482	X	0.7	–	–	–
S5 0836+710	FSRQ	2.172	08 41 24	+70 53 42	391	–	8.5	0.6	–	–
3C 273	Blazar	0.15834	12 29 07	+02 03 09	655	X	35.6	6.0	32	10.6 ± 0.3
3C 279	Blazar	0.53620	12 56 11	+05 47 22	497	X	6.8	–	3	3.3 ± 0.5
PKS 1830–211	Blazar	2.507	18 33 40	–21 03 40	1069	–	16.1	1.4	–	–

[a] ISGRI exposure time

[b] flux in $50 - 150\,\mathrm{keV}$ in units of $10^{-4}\,\mathrm{ph\,cm^{-2}\,s^{-1}}$

[c] tentative redshift

TABLE 3
INTEGRAL AGN FIT RESULTS

Name	ISGRI[a] $f_{20-40\,\mathrm{keV}}$	ISGRI[a] $f_{40-100\,\mathrm{keV}}$	JEM-X[a] $f_{2-10\,\mathrm{keV}}$	$\log L_X$[b] [20 – 100 keV]	$N_{\rm H}$ [10^{22} cm^{-2}]	Γ
NGC 788	2.98 ± 0.24	5.06 ± 0.41	–	43.52	< 0.02[e]	$1.69^{+0.31}_{-0.27}$
NGC 1068	0.93 ± 0.27	1.66 ± 0.48	–	41.92	> 150[n]	$1.71^{+0.82}_{-0.80}$
NGC 1275	1.89 ± 0.21	2.29 ± 0.25	4.34 ± 0.03	43.47	3.75[d]	$2.12^{+0.60}_{-0.43}$
3C 111	6.27 ± 0.57	8.10 ± 0.74	–	44.90	0.634[e]	$2.03^{+0.45}_{-0.37}$
MCG +8-11-11	6.07 ± 0.97	5.80 ± 0.92	–	44.06	< 0.02[f]	$2.41^{+1.24}_{-0.70}$
MRK 3	3.65 ± 0.39	4.62 ± 0.64	–	43.53	110[f]	$2.05^{+0.27}_{-0.23}$
MRK 6	2.01 ± 0.20	2.68 ± 0.26	–	43.57	10[f]	$2.01^{+0.42}_{-0.35}$
NGC 4051	1.80 ± 0.20	1.48 ± 0.17	–	43.60	< 0.01[f]	$2.62^{+0.81}_{-0.53}$
NGC 4151	26.13 ± 0.16	31.97 ± 0.20	20.89 ± 0.01	43.15	4.9[g]	2.10 ± 0.02
NGC 4253	0.93 ± 0.22	1.38 ± 0.32	–	42.93	0.8[f]	$1.85^{+0.78}_{-0.60}$
NGC 4388	9.54 ± 0.25	13.08 ± 0.35	4.63 ± 0.25	43.55	27[h]	$1.92^{+0.09}_{-0.09}$
NGC 4395	0.56 ± 0.22	1.20 ± 0.47	–	40.64	0.15[e]	$1.31^{+0.85}_{-0.71}$
NGC 4507	6.46 ± 0.36	9.11 ± 0.50	–	43.68	29[f]	$1.92^{+0.35}_{-0.31}$
NGC 4593	3.31 ± 0.16	3.39 ± 0.16	2.90 ± 0.89	43.08	0.02[f]	$1.02^{+0.63}_{-0.59}$
Coma Cluster	1.09 ± 0.12	1.00 ± 0.15	8.82 ± 1.27	43.40	< 0.01[d]	$2.65^{+0.18}_{-0.18}$
NGC 4945	9.85 ± 0.23	15.78 ± 0.37	–	42.30	400[f]	$1.93^{+0.09}_{-0.08}$
ESO 323-G077	1.20 ± 0.19	2.03 ± 0.33	–	43.21	55[i]	$1.72^{+0.51}_{-0.33}$
NGC 5033	1.06 ± 0.24	0.84 ± 0.19	–	41.55	2.9[f]	$2.7^{+7.3}_{-1.2}$
Cen A	32.28 ± 0.17	43.79 ± 0.23	29.58 ± 0.02	42.75	12.5[d]	$1.94^{+0.02}_{-0.02}$
MCG-06-30-015	2.98 ± 0.19	3.50 ± 0.22	4.46 ± 0.51	42.93	17.7[f]	$2.04^{+0.10}_{-0.11}$
4U 1344-60	2.83 ± 0.15	3.73 ± 0.20	–	44.36	2.19[f]	$1.65^{+0.02}_{-0.03}$
IC 4329A	8.19 ± 0.17	10.71 ± 0.23	0.98 ± 1.21	44.04	0.42[f]	$2.01^{+0.09}_{-0.08}$
Circinus gal.	10.73 ± 0.18	9.39 ± 0.15	1.29 ± 0.73	41.97	360[f]	$2.74^{+0.09}_{-0.09}$
NGC 5506	4.21 ± 0.33	3.69 ± 0.30	8.87 ± 0.23	42.83	3.4[f]	$2.15^{+0.09}_{-0.08}$
PG 1416-129	5.43 ± 0.64	8.62 ± 1.01	–	45.78	0.09[e]	$1.77^{+0.51}_{-0.41}$
IC 4518	0.49 ± 0.32	1.04 ± 0.68	–	42.92	?	$1.48^{+3.47}_{-1.57}$
NGC 6221	1.32 ± 0.20	1.77 ± 0.27	–	42.39	1[k]	$1.82^{+0.35}_{-0.28}$
NGC 6300	3.91 ± 0.37	3.72 ± 0.35	4.66 ± 1.69	42.36	22[l]	$2.42^{+0.54}_{-0.41}$
GRS 1734-292	4.03 ± 0.09	3.13 ± 0.07	68.4 ± 4.5	43.88	3.7[d]	$2.67^{+0.12}_{-0.11}$
IGR J18027-1455	2.03 ± 0.16	1.66 ± 0.13	4.38 ± 0.31	44.03	19.0[d]	$2.60^{+0.56}_{-0.42}$
ESO 103-G35	2.97 ± 0.66	5.27 ± 1.17	–	43.51	13 – 16[e]	$1.64^{+0.97}_{-0.70}$
1H 1934-063	0.48 ± 0.25	0.83 ± 0.44	–	42.51	?	$2.92^{+0.81}_{-0.63}$
NGC 6814	2.92 ± 0.23	2.64 ± 0.21	–	42.52	< 0.05[e]	$2.48^{+0.49}_{-0.36}$
Cygnus A	3.24 ± 0.14	3.55 ± 0.15	–	44.71	20[m]	$2.24^{+0.19}_{-0.17}$
MRK 509	4.66 ± 0.47	4.96 ± 0.50	4.56 ± 0.78	44.42	< 0.01[f]	$1.73^{+0.15}_{-0.16}$
IGR J21247+5058	4.15 ± 0.27	6.85 ± 0.45	–	44.00[c]	?	$1.73^{+0.24}_{-0.22}$
MR 2251-178	1.20 ± 0.17	1.27 ± 0.18	–	44.40	0.02 – 0.19[e]	$2.31^{+1.21}_{-0.68}$
MCG -02-58-022	1.20 ± 0.28	1.75 ± 0.41	–	44.18	$< 0.01 - 0.08$[e]	$1.71^{+0.89}_{-0.63}$
S5 0716+714	0.14 ± 0.11	0.71 ± 0.59	–	45.21[c]	< 0.01[e]	–
S5 0836+710	1.73 ± 0.28	3.02 ± 0.50	–	47.87	0.11[e]	$1.65^{+0.46}_{-0.39}$
3C 273	5.50 ± 0.15	6.29 ± 0.17	9.21 ± 0.29	45.92	0.5[d]	$2.17^{+0.12}_{-0.12}$
3C 279	0.82 ± 0.24	1.79 ± 0.52	6.05 ± 2.36	46.37	$0.02 - 0.13$[e]	$1.3^{+0.7}_{-0.5}$
PKS 1830–211	2.07 ± 0.14	2.82 ± 0.19	–	48.09	$< 0.01 - 0.7$[e]	$1.96^{+0.27}_{-0.24}$

[a] flux in $10^{-11}\,\mathrm{erg\,cm^{-2}\,s^{-1}}$

[b] uminosity in $\mathrm{erg\,s^{-1}}$ for $H_0 = 70$ and $\Lambda_0 = 0.73$

[c] tentative redshift

[d] this work, [e] Tartarus database, [f] Lutz et al. 2004, [g] Beckmann et al. 2005, [h] Beckmann et al. 2004, [i] Sazonov & Revnivtsev 2004, [k] Levenson, Weaver & Heckman 2001, [l] Matsumoto et al. 2004, [m] Young et al. 2002, [n] Matt et al. 1997a

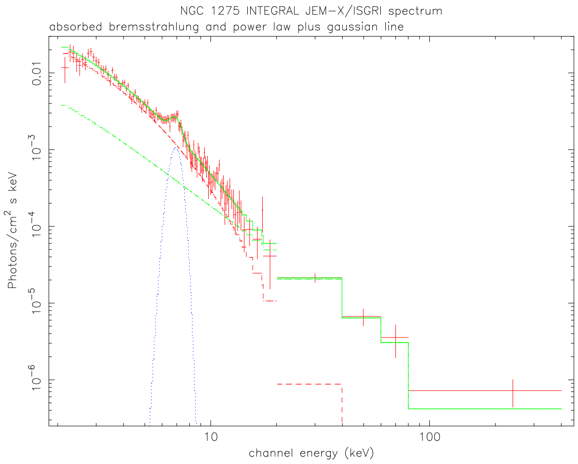

Fig. 1.— *INTEGRAL* spectrum of NGC 1275.

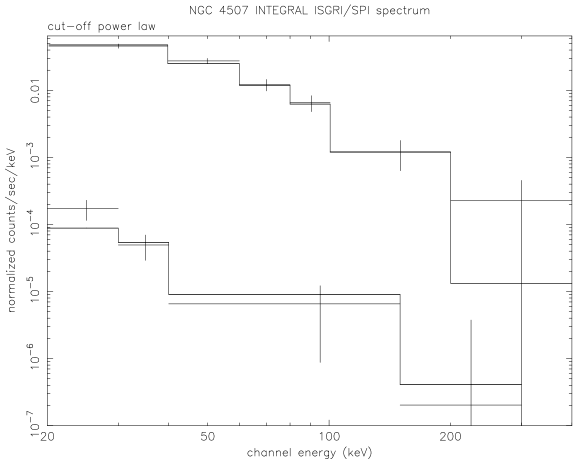

Fig. 2.— *INTEGRAL* count spectrum of NGC 4507. No JEM-X data are available for this source. We note that here, and elsewhere SPI spectral data are presented, the "detector counts" have really been effective area corrected by the image reconstruction algorithm (Skinner & Connell 2003). Thus, the SPI spectra are really photons $\mathrm{cm}^{-2}\,\mathrm{s}^{-1}\,\mathrm{keV}^{-1}$.

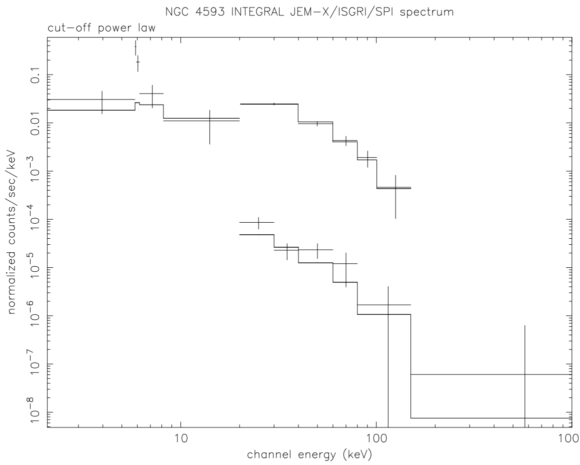

Fig. 3.— *INTEGRAL* count spectrum of NGC 4593.

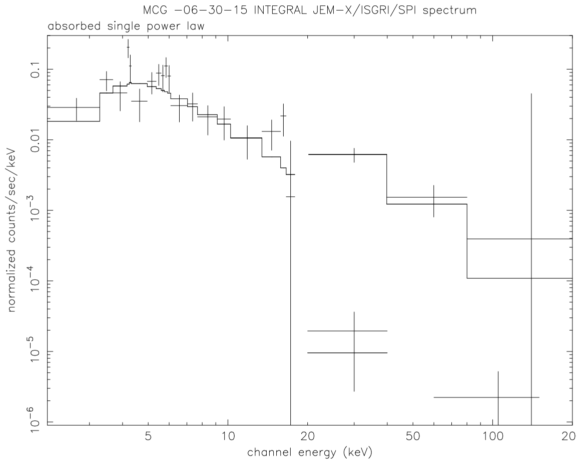

Fig. 4.— *INTEGRAL* count spectrum of MCG –06–30–015 with JEM-X (2 – 18 keV), ISGRI (20 – 200 keV; upper spectrum), and SPI (lower two points).

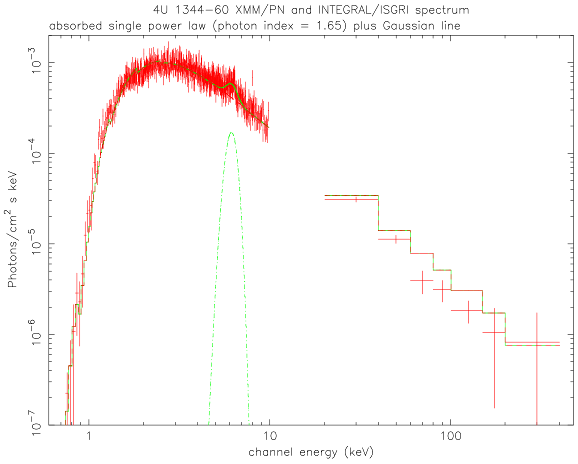

Fig. 5.— Combined XMM-Newton EPIC/pn and *INTEGRAL* ISGRI photon spectrum of 4U 1344–60. The SPI spectrum is not shown for better readability. The iron Kα line indicates a redshift of about $z = 0.043$.

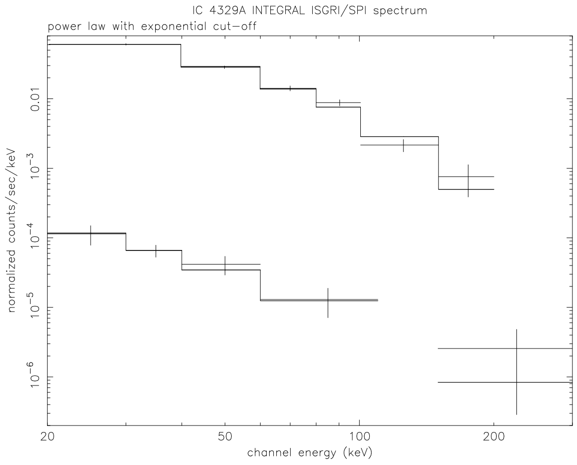

Fig. 6.— *INTEGRAL* ISGRI and SPI count spectrum of IC 4329A.

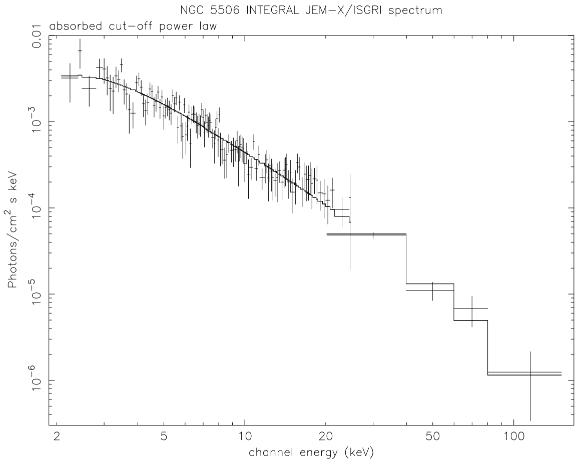

Fig. 7.— *INTEGRAL* spectrum of NGC 5506.

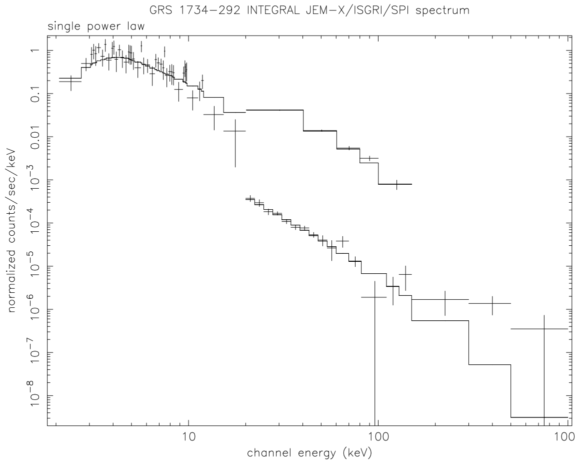

Fig. 8.— *INTEGRAL* count spectrum of GRS 1734–292.

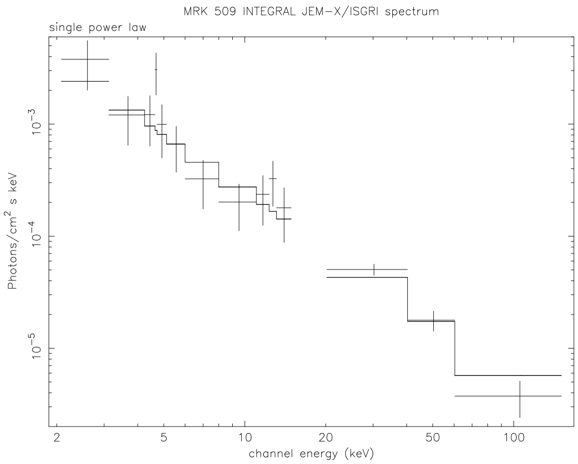

Fig. 9.— *INTEGRAL* spectrum of MRK 509. No SPI data are available for this source.

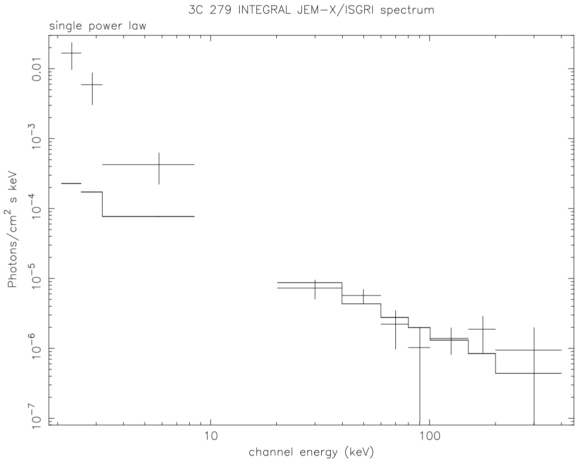

Fig. 10.— *INTEGRAL* spectrum of the blazar 3C 279. The source is not detectable in the SPI data.

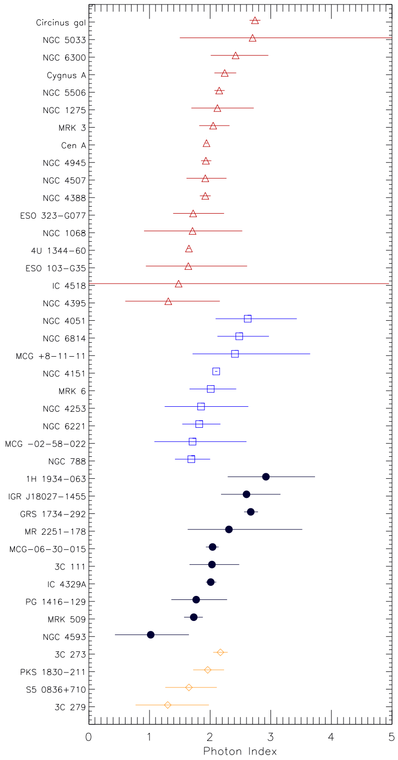

Fig. 11.— Photon index of a single power law fit to the *INTEGRAL* data of our sample, ordered in four categories. From top to bottom: Seyfert 2, Seyfert 1.5, Seyfert 1, and blazars.

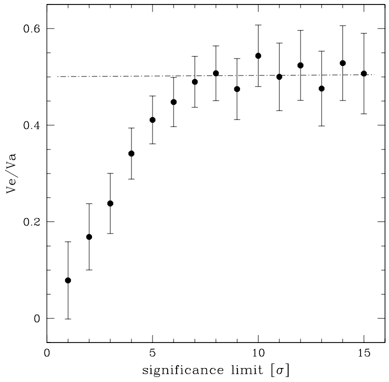

Fig. 12.— Result of the V_e/V_a-test assuming different completeness limits in ISGRI significance. The dashed dotted line shows the average $\langle V_e/V_a \rangle$ value for the objects with significance $\geq 7\sigma$.

Table 2: *CGRO*/OSSE detected AGN not seen by *INTEGRAL*

Name	Type	exposure[a] [ks]
3C 120	Sy1	3
3C 390.3	Sy1	–
3C 454.3	blazar	2
CTA 102	blazar	6
ESO 141-G55	Sy 1	23
H 1517+656	BL Lac	2
III Zw2	Sy1/2	79
MRK 279	Sy1.5	13
MRK 841	Sy1.5	–
M82	Starburst	84
NGC 253	Starburst	–
NGC 2110	Sy2	–
NGC 3227	Sy1.5	–
NGC 3783	Sy1	–
NGC 526A	Sy1.5	–
NGC 5548	Sy1.5	–
NGC 7172	Sy2	–
NGC 7213	Sy1.5	–
NGC 7314	Sy1.9	489
NGC 7469	Sy1.2	2
NGC 7582	Sy2	–
PKS 0528+134	blazar	1040
PKS 2155-304	BL Lac	–
QSO 1028+313	Sy1.5	–

[a] ISGRI exposure time

Table 4: Cut-off power law fits

source	Γ powerlaw	E_C [keV]
NGC 4507	$1.0^{+1.7}_{-0.8}$	55^{+123}_{-11}
NGC 4593	$1.02^{+0.63}_{-0.59}$	35^{+49}_{-12}
ESO 323-G077	$1.48^{+0.65}_{-1.18}$	181^{+319}_{-131}
IC 4329A	$1.51^{+0.39}_{-0.40}$	104^{+344}_{-48}
Circinus Galaxy	$2.23^{+0.48}_{-0.55}$	$87^{+\infty}_{-46}$
NGC 5506	$1.81^{+0.25}_{-0.28}$	57^{+139}_{-27}

Table 5: Average spectra

source type	Γ^a
unabsorbed Sy	2.08 ± 0.02
absorbed Sy	1.98 ± 0.01
Seyfert 1	2.11 ± 0.05
Seyfert 1.5	2.10 ± 0.02
Seyfert 2	1.95 ± 0.01
Blazar	2.07 ± 0.10

[a] weighted mean of the individual source results